Journal of Solid State Chemistry 338 (2024) 124820

Contents lists available at ScienceDirect

Journal of Solid State Chemistry

journal homepage: www.elsevier.com/locate/jssc

Controlling ZIF-67 film properties in water-based cathodic electrochemical deposition

Eman Elsayed [a,*], Ignacio Brevis [b], Sathish Pandiyan [c], Ricky Wildman [c], Kristoffer G. van der Zee [b], Begum Tokay [a,**]

[a] Department of Chemical and Environmental Engineering, Faculty of Engineering, University of Nottingham, University Park, NG7 2RD, UK
[b] School of Mathematical Sciences, University of Nottingham, Nottingham, NG7 2RD, UK
[c] Centre for Additive Manufacturing, Faculty of Engineering, University of Nottingham, Nottingham, NG7 2RD, UK

ARTICLE INFO

Keywords:
Electrochemistry
Cathodic electrodeposition
MOFs
ZIF-67

ABSTRACT

One of the main approaches to increase the surface area of a substrate is through depositing a film of a porous materials such as Zeolite imidazole framework (ZIF). ZIF films have shown surpassing capabilities because of their zeolite-like features, including porosity, homogeneous pore size, structural tunability and remarkable thermal and chemical stability. Many methods have been proposed and tested to form such films. One of the techniques that have been documented is electrosynthesis which is considered to be the most practical, quick, and mildly conditioned.

In this study, ZIF-67 films were cathodically electrodeposited on an electrically conductive Indium Tin Oxide (ITO) coated Polyethylene Terephthalate (PET) substrates. Unlike previous reports, in this study, water was used as a solvent. In addition to this, effect of crucial operating parameters such as applied potential, molar ratio of reactants and solution pH, on the formation of ZIF-67, was investigated for the first time. It was found that increasing the applied potential, increased the surface coverage and decreased the formed ZIF-67 crystal size. Changing the molar ratio between the organic ligand and the metal salt had a profound influence on the formed phase and crystal shape. It was also found that at neutral and mildly basic solution pH, ZIF-67 could not be formed. Also, statistical analyses were carried out showing low p-values ($\ll 0.05$), expressing strong relation between variables and robustness and reliability of the data collected in this study. Finally, mathematical expressions were fitted to experimental data to reveal the relation between applied potential, molar ratios of reactants, pH and conductivity of solutions, surface coverage and crystal size.

This study revealed that surface coverage, crystal shape and size can be controlled by manipulating operating conditions.

1. Introduction

Zeolitic imidazolate frameworks (ZIFs) are a subfamily of metal-organic frameworks (MOFs). Many techniques have been used to produce MOFs such as microwave assisted, sonochemical, mechanochemical, hydrothermal and solvothermal methods [1–6]. In particular, ZIFs mirror zeolite type topology because of their huge surface areas, adjustable pore apertures, and microporous structure, they have outstanding thermal and chemical stability [7,8]. Cobalt-based zeolitic imidazolate framework, known as ZIF-67, is formed by bridging 2-methylimidazolate anions and cobalt cations within a sodalite zeolite-type topology [9,10] (Fig. 1). It has a high surface area (>1700 $m^2\ g^{-1}$) with micropores (0.34 nm) and strong affinity for guest molecules [11]. Due to such properties, ZIF-67 is a suitable fit for a number of applications such as adsorption and detection of volatile organic compounds (VOCs), gas separation, supercapacitors, catalysis, gas storage, carbon capture and pyrolysis [12–19]. But even while they seem practical and promising from an industrial standpoint, they don't always meet all the requirements for the purposes for which they were designed. This is frequently due to being synthesized in micron size crystalline powders [20]. Thin films seems to the solution for such problem.

Nevertheless, numerous expected uses, include thin films in sensor

* Corresponding author.
** Corresponding author.
E-mail addresses: eman.hussein@nottingham.ac.uk, eng.eman.m.elsayed@gmail.com (E. Elsayed), begum.tokay@nottingham.ac.uk (B. Tokay).

https://doi.org/10.1016/j.jssc.2024.124820
Received 10 April 2024; Received in revised form 24 May 2024; Accepted 6 June 2024
Available online 15 June 2024

devices or gas separation membranes, require deposition of ZIFs on different surfaces that presents serious challenges [21]. Many factors make porous coatings desirable e.g., pre-loading particles or molecules into the pores can alter the surface's optical (dyes), catalytic (particles/molecules), and tribologic (lubricants) capabilities. As an alternative, the coating itself may function as a host for external molecules, acting as a filter or a membrane [22–27]. Several techniques have been developed for the production of films, including spin coating, gel layer synthesis, liquid phase epitaxial deposition, layer-by-layer deposition, chemical vapour deposition and electrosynthesis. However, the majority of these techniques are complicated, time and energy consuming, and creating a reliable and straightforward MOF deposition process is still difficult [28–30]. The deposited films are never inter-grown, and surface adhesion is frequently poor [31,32]. Also, most ZIFs membranes/films are kept thicker than microns in order to prevent separation layer flaws. However, the greater the thickness, the lower the molecule flow, which is not favourable for industrial purposes [33]. Few studies have been conducted on the synthesis of thin ZIF-67 films. This is mostly due to the fact that ZIF-67 exhibits extremely easy homogeneous nucleation in solution and very low heterogeneous nucleation density on the substrate, which makes it difficult to manufacture ultra-thin and flawless ZIF-67 films [33].

Another challenge is that it has been reported to be synthesized using various solvents such as DMF, acetonitrile, methanol or their mixtures [9,34–37] at elevated temperatures (50 and 200 °C) [11]. These organic solvents have a high cost and are hazardous. Furthermore, it might be difficult to exclude some organic solvents from MOFs and ZIFs' pores (e.g., DMF) [38].

Recently, electrochemical deposition has been suggested as a viable and practically applicable method for in situ patterning and deposition on conductive surfaces [31]. This is due to the electrochemical synthesis being convenient, fast, offering controlling the thickness and morphology by altering applied current or voltage [21,22,39,40], allows the deposition under mild conditions such as atmospheric pressure and ambient temperature, may not require pre-treatment of the support and has potential for large-scale production [29,30,32,41,42].

In electrosynthesis and as a result of the metal ions being created in situ close to the support surface, there is less crystallization in the bulk phase, which should prevent unwanted crystals piling up throughout the film synthesis process. In addition to this, because thermally induced film cracks during cooling should be less noticeable (in comparison to solvothermal synthesis), using lower temperatures are thought to be advantageous. Compared to solvothermal approaches, electrochemical synthesis methods provide extra parameters for fine-tuning since they allow the imposition of particular signals or voltage adjustments [39]. ZIF-67 can be electrodeposited by a cathodic [36] or anodic [43] processes. In the latter, metal ions are produced by the substrate dissolving anodically (cobalt in case of ZIF-67), which imposes limitations on the substrate [44]. In cathodic deposition, the reduction of pro-bases such as nitrate anions and the ensuing deprotonation of the linkers are what cause the pH to rise close to the working electrode, which is necessary for cathodic deposition. Consequently, cathodic deposition can employ a far larger variety of substrates [22,29].

Previous studies showed that ZIF-67 electrodeposition was limited to deposition on a few substrates such as Copper mesh/foam, Fluorine Tin Oxide (FTO) glass, Nickel foil/foam, Titanium foil, ITO/PET, and stainless-steel mesh using methanol/water as a solvent at specific potentials [35,36,45]. However, these studies have not evaluated the deposition parameters in depth or using greener approaches for synthesis.

In this study we report the effect of operating parameters such as applied potential, reactants molar ratio and solution pH on the deposition and morphology of ZIF-67 films and crystals. This study adapted a more environmentally friendly approach to develop ZIF-67 films without using any organic solvents. To the best of our knowledge, there is no comprehensive study on the electrodeposition of ZIF-67 on conductive substrates (e.g., ITO/PET) using water as a solvent and how it might affect the integrity of the electrochemically formed film.

Results showed that increasing the applied potential, increased the surface coverage and decreased the ZIF-67 crystal size. Changing the molar ratio between the organic ligand and the metal salt had a profound influence on the formed phase and crystal shape. It was also found that at neutral and mildly basic solution pH, ZIF-67 could not be formed.

Statistical study revealed that the p-values calculated in this study is statistically significant in such case the null hypothesis is rejected. This means that there is much less than a 5 % chance that the strength of the relation between the variables proposed in this study might have happened by chance proving the strong relation between variables, robustness and reliability of the data collected in this study. Also, mathematical expressions were presented to fit experimental results and show the relation between applied potential, reactants molar ratios, solution pH, solution conductivity, surface coverage and crystal size.

All the coated substrates and their corresponding powders were characterized using X-ray diffraction (XRD), Scanning Electron Microscopy (SEM), X-ray Photoelectron Spectroscopy (XPS) and Fourier transform infrared (FTIR) spectroscopy to evaluate the structure, morphology and the surface coverage of the films.

2. Methodology

2.1. Materials

Indium Tin Oxide coated Polyethylene Terephthalate (ITO/PET) sheets (Surface resistivity = 100 Ω, thickness = 0.127 mm), platinum wire (thickness = 0.8 mm, length = 4 cm), cobalt nitrate hexahydrate ($Co(NO_3)_2{\cdot}6H_2O$) (98 %) and 2-methylimidazole (HMim) (99 %) were purchased from Sigma-Aldrich. Chemical reagents were used without further treatments. De-ionized water (18.2 MΩ cm resistivity, Milli-Q®-IQ 7015 Ultrapure lab) was used as solvent.

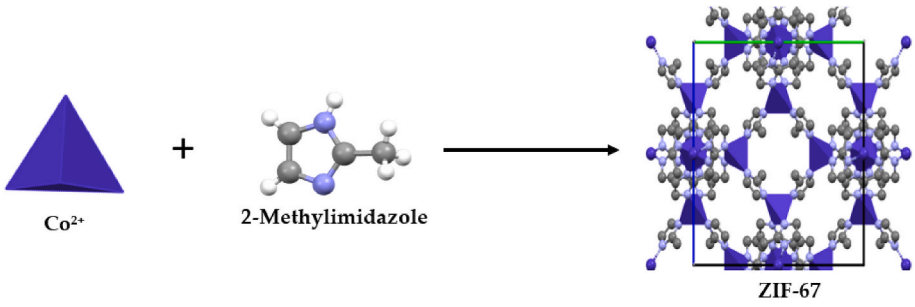

Fig. 1. The ZIF-67 crystal structure and its building blocks.
(The atoms highlighted are: hydrogen as white, carbon as grey, Nitrogen as light purple, cobalt as dark purple).

2.2. Synthesis and characterization of ZIF-67 coatings/films on ITO/PET substrates

Prior to experiments, ITO/PET substrates were successively washed using acetone and deionized water. Electrodeposition was carried out in a three-electrode electrochemical cell where the ITO/PET, Ag/AgCl and platinum wire were the working, reference, and counter electrodes, respectively (Fig. S1, Supplementary Information). Substrates with the surface area of 1×4 cm^2 were used for all the experiments. The initial reactant concentrations were adopted from Ref. [46]. The parent electrolyte solution was 10 ml 0.099 M $Co(NO_3)_2{\cdot}6H_2O$ and 40 ml 1.75 M HMim. The effect of applied potential was investigated in the range of −0.25 to −0.8 V. The cycle time was set to 10 min. The effect of solution pH on deposition was determined by adjusting the original solution pH in the range of 7–12.5 by using concentrated HNO_3 acid (70 % v/v) or 10 M NaOH. Volumes of NaOH solution and HNO_3 acid used are shown in (Table S1). After electrodeposition, the obtained ZIF-67@ITO/PET films were rinsed with water and left to dry in air at room temperature. The effect of linker/metal molar ratio on deposition was investigated by changing the ratio in the range of 1–70. This was achieved by maintaining metal salt (0.099 M) or HMim (1.75 M) concentrations constants, respectively, while changing the other and monitoring the pH of the solution for each set (Table S2 and Fig. S2). To further determine whether linker/metal ratio or pH of the solution has more pronounced effect on the formation of ZIF-67 films, experiments were repeated for the of molar ratio = 1 (MR1) and molar ratio = 16 (MR16) (fixed cobalt concentration = 0.99 M) after re-adjusting the solution pH. Volumes of NaOH solution and HNO_3 acid used are shown in Table S4.

XRD patterns were measured using Bruker D8 Advance Diffractometer with Cu Kα radiation (1.54056 Å). Due to the characteristic peaks of ITO/PET substrate coinciding between 17 and 30° 2θ (overwhelming the peaks of ZIF-67), coated film samples were scanned from 4 to 16° 2θ with a step size of 0.05° and was spun at 15 rpm while powder samples were scanned from 4 to 50° 2θ.

SEM images were collected using JEOL 7000F at 15 kV. Samples were coated with an 8 nm Iridium layer prior to analysis. ImageJ software was used to calculate the surface coverage and crystal size.

Transmission FTIR spectra were collected using Bruker Tensor 27 between 400 and 4000 cm^{-1}.

XPS spectra were collected using Thermo Fisher K-Alpha photoelectron spectrometer. The spot size used was 400 μm and the power settings were 12 kV, 6 mA. The charging was corrected by cantering the C–C peak near 284.8 eV. CasaXPS software was used to process the data [47].

A statistical analysis (Supporting **Information**) was carried out in which standard deviations were calculated and included with all data presented in the current study. Also, Pearson and Spearman correlations along with their associated p-values were calculated to describe the strength and direction of an association between variables. Finally, mathematical expressions were fitted to experimental data to reveal the relationship between applied potential, molar ratios of reactants, pH and conductivity of solutions, surface coverage and crystal size.

3. Results and discussion

3.1. Advantage of electrochemical deposition

The advantage of electrochemical deposition over the room temperature natural deposition was investigated through carrying out two deposition experiments. The first experiment was the cathodic electrodeposition in which a potential of −0.5V was applied for 1 h in the three electrodes cell using the standard ZIF-67 solution. The other experiment was carried out exactly the same but without applying any current but only through immersing the ITO/PET substrate in the reaction solution. This experiment was labelled as natural deposition. A schematic showing the two experiments is shown in Fig. 2.

Fig. 3 illustrates the XRD of ZIF-67 film formed on substrates from both experiments; the formation of ZIF-67 crystals was confirmed through the presence of the characteristic peak at 7.3°.

Fig. 4 shows the SEM images of both substrates where it can be noticed that the electrodeposition technique enabled the formation of ZIF-67 along the substrate without the formation of agglomeration

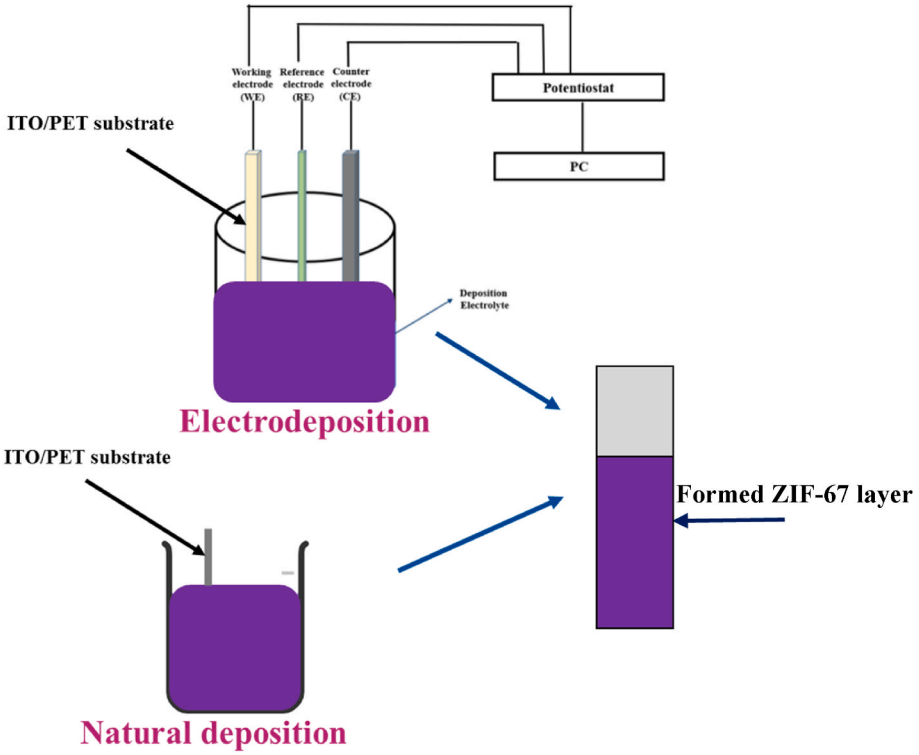

Fig. 2. Schematic of the three-electrode electrochemical cell and natural deposition for the fabrication of ZIF-67 coating on ITO/PET substrate.

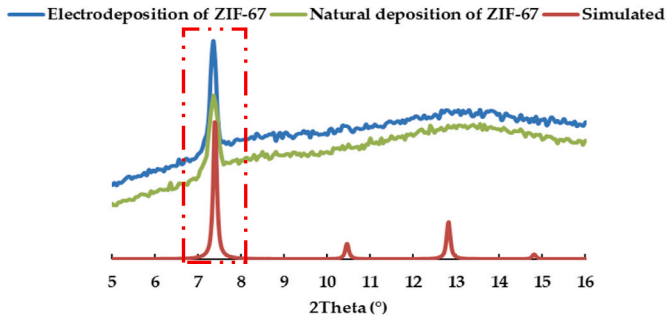

Fig. 3. XRD of electrochemical deposition at −0.5V and natural deposition of ZIF-67 on ITO/PET substrates after 1 h.

unlike the natural deposition where agglomeration can clearly be seen. An average coverage of 49 % was noticed for the electrodeposition compared to 43 % in case of natural deposition. The crystal size was slightly smaller in case of electrodeposition as it was 0.42 μm compared to 0.48 μm in case of natural deposition which is in good agreement with previously ZIF-67 crystals obtained in methanol with a size of 500 nm. This experiment highlights the advantage of electrochemical deposition which is the uniform higher surface coverage.

To ensure the consistency and reliability of the three-electrode electrodeposition system, all the reported data were repeated for three times. Average values with standard deviation were reported. An example of data repeatability is shown in Fig. 5 in which three tests were performed at the same operating conditions (−0.5 V for 1 h). The average surface coverage in the three tests was found to be 49 % with a standard deviation of ±0.28 and the average crystal size was 0.42μm with a standard deviation of ±0.056. The current transient plot shown in the figure shows that the current density variation with time is repeatable with small deviation proving the repeatability, consistency and reliability of the data collected in this study.

3.2. Effect of applied potential

Applied potential is considered as one of the most influential parameters as it does not only affect the rate of the MOF/ZIF-67 formation, but also the nature of the deposited materials. High potential can lead to the deposition of cobalt metal or changes in the nature of the substrate. When using ITO/PET as a working electrode and cobalt nitrate hexahydrate as the source of cobalt, the electrodeposition of cobalt metal was determined around −0.9 V. To avoid the deposition of the cobalt metal, the effect of the applied potential was investigated up to −0.8 V to investigate its effect on the surface coverage and crystallinity. Experiments were also conducted at potentials above −0.8 V to investigate the deposition of ZIF-67 on the substrate.

The growth and nucleation kinetics of ZIF-67 can be understood form Fig. 6 which shows the current transient plot at applied potentials from −0.25 to −0.8V. For all applied potentials, it can be noticed that after the double layer charging step, a rapid change in the current density was observed. This change corresponds to the nucleation step and the

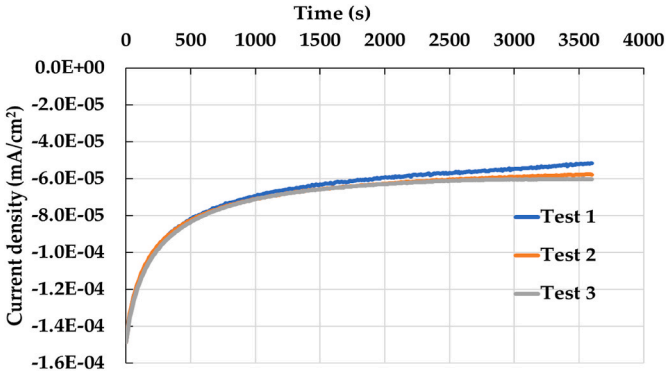

Fig. 5. Current transient plot for repeatability test at −0.5V for 1 h.

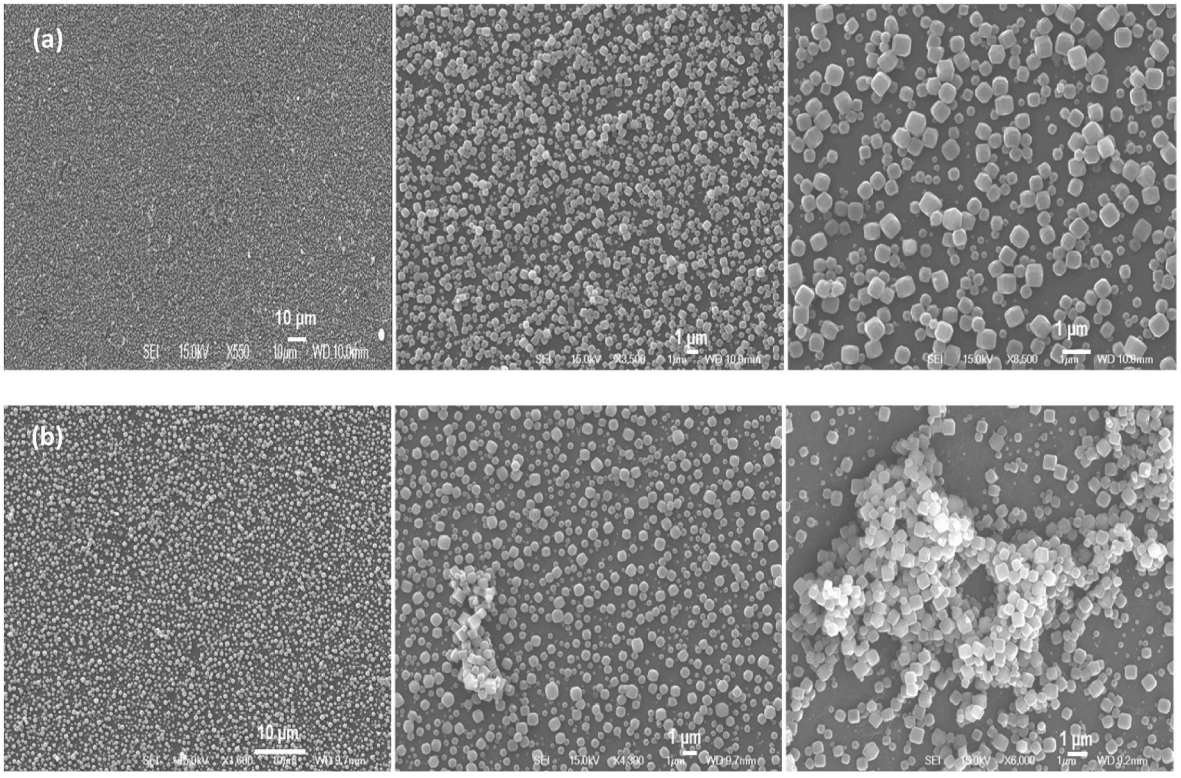

Fig. 4. SEM images of a. Electrodeposition at −0.5V and b. Natural deposition of ZIF-67 on ITO/PET substrates after 1 h.

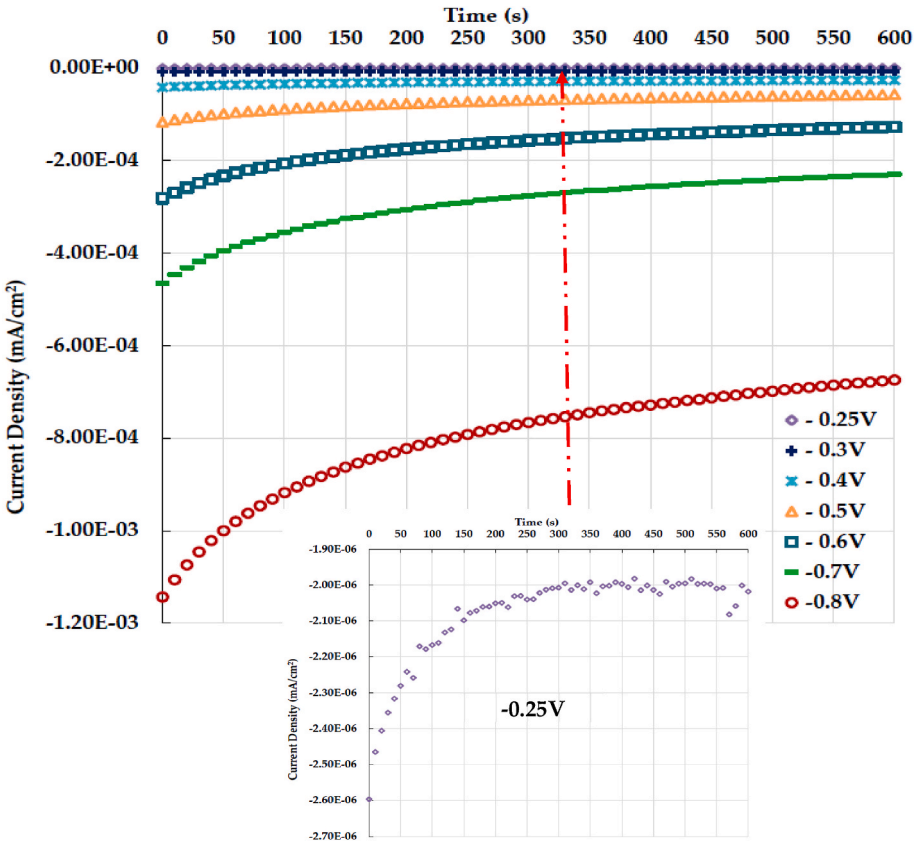

Fig. 6. Current transient plot at applied potentials from −0.25 to −0.8V for 10 min.

number of nuclei formed.

It can be also noticed that at t = 5 min (300 s), 80 % of the equilibrium current density values were reached. As the electrodeposition time increases, the last change in the current density is observed where it reaches almost a plateau. In this stage progressive nucleation is taking place in which simultaneously nuclei are formed along with crystal growth of the formed ZIF-67 nuclei into a thin film. The slow growth is due to the species linear diffusion from the bulk electrolyte to the electrolyte/electrode interface. In this stage, the concentration of the ions decreases in the compact layer adjacent to the electrode surface and the reaction becomes limited to the mass transfer of the ions from the bulk solution to the electrode surface and thus the current density reaches a plateau (Fig. S7).

It was also noticed that as the applied potential was increased from −0.25 to −0.8 V, the equilibrium current density changed from -2E-6 to −6.7E-4 mA cm^{-2}. This may be the result of high electroactive area with the raising of nuclei numbers due to the higher ion concentrations at the beginning of the deposition as higher applied voltage permits higher electrons flow. The rate of the change in current density was calculated and presented in Fig. S8 which showed a dramatic change as the applied potential decrease. This change corresponds to the rate of the electron generation with the solution. This rate drastically decreases with time till a near steady state is reached almost at 300 s.

The effect of applied potential on the crystallinity of the deposited crystals is shown in Fig. 7. ZIF-67 crystals were successfully formed at all the applied potentials as evident from the characteristic peak at 7.3° which is good agreement with previous studies [48]. As the applied potential was increased from −0.25 V to −0.8 V or further to −5 V, the intensity of the peak at 7.3° increased, which might be attributed to the higher surface coverage and higher amount of electrodeposited ZIF-67.

The effect of applied potential on the morphology of the deposited ZIF-67 crystals was determined via SEM images (Fig. 8 and Fig. S9). Changing the potential from −0.25 V to −0.8 V, increased the surface coverage from 19.7 % ± 1.45 to 45.6 % ± 0.68 while it decreased the average crystal size from 0.52 ± 0.1 μm to 0.29 ± 0.1 μm (Fig. 8). At higher applied potentials (>-0.8 V), the rate of electrons released increased, which may have further increased the nucleation rate and the formation of smaller crystals (Fig. S9). A similar behaviour was observed with $Zn_3(BTC)_2$ and $Cu_3(BTC)_2$ (HKUST-1) films, which were grown via anodic electrodeposition. These results showed that increasing the voltage sped up the production of metal ions on the surface of the electrode and the migration of linker ions, which favoured the growth of MOF films by offering more nucleation sites [49–51]. Further increase in the potential from −0.8 V to −5 V increased the surface coverage to 78 ± 0.45 % but did not change the average crystal size (0.28 ± 0.1 μm) (Fig. 8). Both figures also show that increasing the applied potential dramatically increased the surface coverage but also increased the numbers of crystal layers formed. This may be attributed to the that at a potential > −0.8 V, there was excessive ion generation and nucleation during the nucleation and growth steps allowing the coverage of the substrate and crystals start building up on top of each other.

Fig. S10 shows the FTIR spectrum of ZIF-67 deposited at various applied potentials. All the main bands of ZIF-67 were observed at all the investigated potentials. In addition, as the potential was increased, bands at 2220 cm^{-1} 1170 cm^{-1} and 424 cm^{-1}, corresponding to C═N bonds, stretching vibration of C–N and Co–N [52,53], respectively became stronger.

Fig. S11 shows the changes taking places to the substrate when high potential was applied. Dark brown marks started to appear in case of -2V, −3 V and −5 V. This is attributed to the electrochemical instability of ITO at higher cathodic potentials (>−0.8 V), resulting in metal cation reduction and gradual decay in its optical and electrical properties which can eventually lead to the electrode's total failure [54]. Regarding the results presented so far, −0.8 V was selected as the optimum potential.

X-ray photoelectron spectroscopy (XPS) tests were performed to

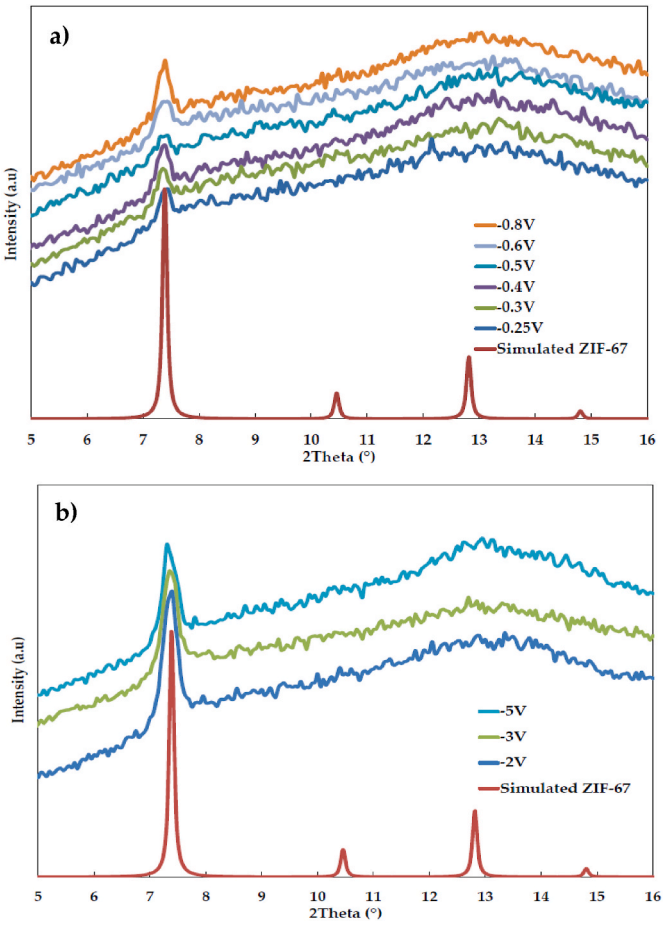

Fig. 7. X-Ray Diffraction (XRD) patterns of ZIF-67 films at applied potentials between a. −0.25 to −0.8 V; and b. −2 to −5 V for 10 min.

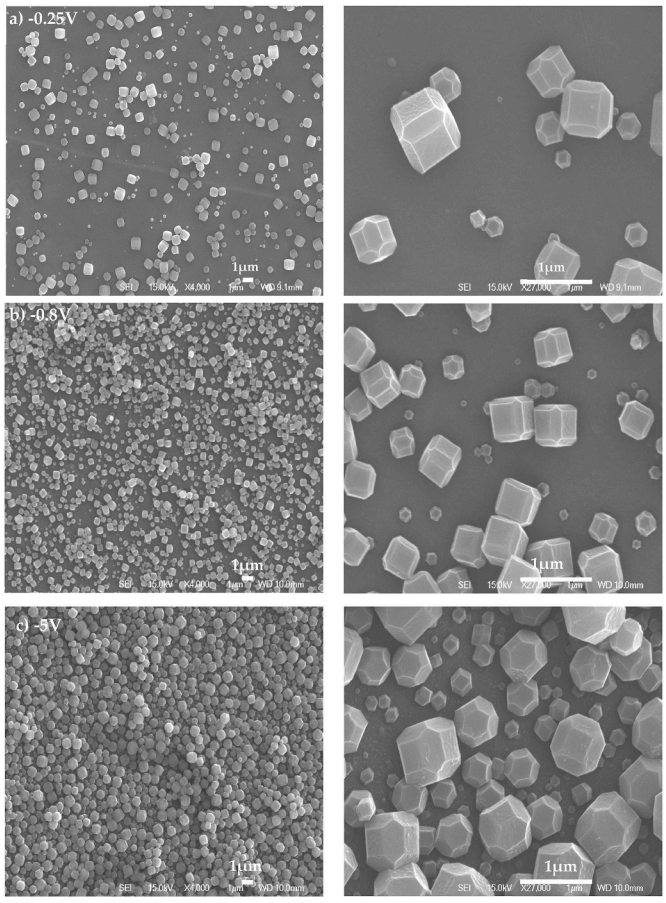

Fig. 8. SEM images of ZIF-67 films at potentials a. −0.25 V, b. −0.8 V, c. −5 V for 10 min.

examine the surface composition and chemical species of the electrodeposited ZIF-67 films. Fig. 9 shows the wide scan and high-resolution scans of Co, N, C and O of the ZIF-67 film developed at −0.8 V for 10 min. The high-resolution XPS spectrum for C 1s was attributed to 4 peaks at 284.5, 285.2, 286.8 and 288.5 eV, corresponding to binding energies (BE) of carbon in a functional groups sp2-C, C–N, N–C═O, and C═O, respectively. The fitted N 1s spectra was attributed to 4 peaks at 398, 398.8, 399.7, 400.7 that corresponds to binding energies (BE) of nitrogen in a functional groups of pyridinic, Co–N, pyrrolic, and graphitic nitrogen, respectively. The formation of the Co–N bond is a characteristic feature for the formation of ZIF-67 as indicated from FTIR spectrum. The XPS spectrum of Co $2p_{3/2}$ was segmented into 4 peaks, representative of Co^{3+} (780.6 eV), Co^{2+} (780.5 eV), Co–Nx (783.7 eV), and satellite (786.7 eV). Thus, the XPS result confirms the coexistence of cobalt and nitrogen bond in the well-structured ZIF-67.

The O 1s can be deconvoluted into four different contributions at 529.2, 530.5, 531.5 and 533 corresponding cobalt oxygen bond, C–OH (hydroxyl), C–O–C (epoxy), and carbonate structures, respectively. The obtained spectrum is in good agreement with the previous studies [55, 56]. The wide scan XPS spectra of the electrodeposited ZIF-67 films at different applied potentials are shown in Fig. S12. It is evident that as the applied potential increases from −0.25V to −0.8V, the Co 2p becomes more profound. This is due to the higher coverage and higher active mass of ZIF-67 electrodeposited on the ITO/PET substrate. With increasing the applied potential to -5V, it can be noticed that peaks corresponding to Tin (Sn 3d and 3p) and Indium (3d and 3p) which can be found in the conducive ITO layer became much weaker. This indicates the higher coverage with the ZIF-67 layer that overwhelms the ITO layer spectrum.

3.3. Effect of molar ratio (MR)

Fig. 10 shows the effect of increasing the linker/metal molar ratio on the crystallinity of both the formed ZIF-67 film and powder samples. From Fig. 10a and c, it can be noticed that the characteristic peaks were only detected for the films at molar ratios of 8.8 and 16, hence powder samples were collected after experiments for XRD analyses. From Fig. 10b and d, it can be noticed that the ZIF-67 characteristic peaks were observed for the powder samples at MR ≥ 8.8 for both concentrations (HMim = 1.75 M and $Co(NO_3)_2$ = 0.099 M) and at MR ≥ 6 at constant HMim concentration.

The other characteristic peaks appearing after 10° in case of MR 4 and 6 for cobalt nitrate concentration of 0.099 M, could be related to diffraction from different planes due to shape as the SEM confirms this as crystals are longer.

Fig. S2 and Table S2 show that as the molar ratio was increased, the pH increased whilst the conductivity decreased. This is due to the higher HMim concentration, which has a higher pH and a lower conductivity, compared to cobalt nitrate. At low concentrations of HMim and lower pH, the ligand is partially deprotonated such that it cannot readily form extended 3D networks [57]. This justifies why no ZIF-67 was formed at low molar ratios between the ligand and the metal salt.

The effect of the molar ratio (at HMim concentration = 1.75 M) on the morphology of the deposited ZIF-67 crystals was also examined via SEM images (Fig. 11, Fig. S15), where it is evident that the molar ratio has a profound effect on the shape of the formed crystals. It can be noticed that MR 1, 4 and 6 yielded rod (0.16 μm), octahedron (1.2×1.5 μm) and spherical (0.85 μm) crystals, respectively. On the other hand, further increase in molar ratio produced dodecahedron crystals (sizes are shown in Table 1). This suggests that molar ratios of 1,4 and 6 was

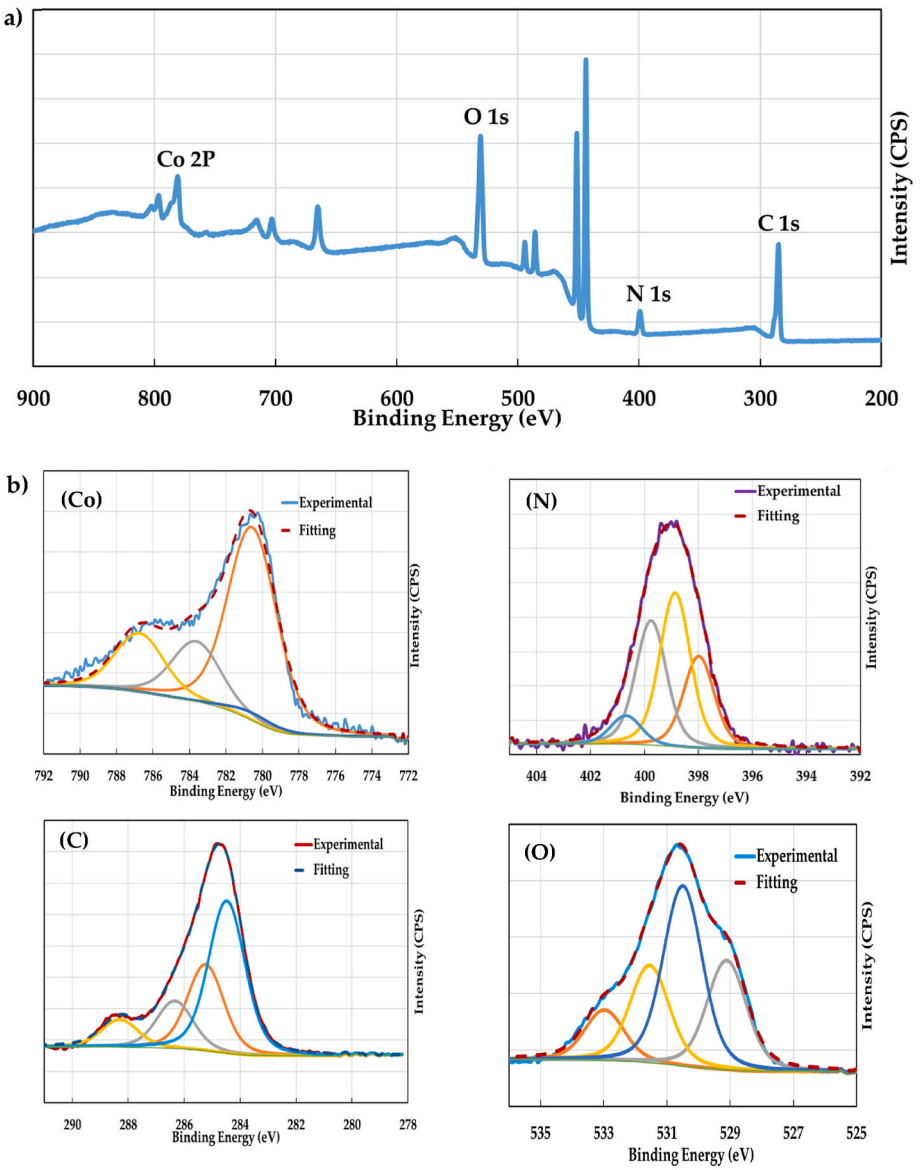

Fig. 9. XPS survey spectrum (a. wide scan and d. high-resolution scans of Co, N, C and O) of electrodeposited ZIF-67 film developed at −0.8 V for 10 min.

not high enough to exhibit the characteristic dodecahedral crystal shape of ZIF-67, which only formed at MR $\geq$ 8.8. This can be attributed that the morphology of the crystals depends on the concentration of the reactants as it affects the nucleation and growth rates [58].

Previous studies on ZIF-8 concluded that 2-methylimidazole should be present in excess even though the reactants (Zn/HMim) should have a reaction stoichiometry ratio of 1:2. This might be attributed to its alkalinity, 2-methylimidazole at high concentrations can be considered as a deprotonation agent. This caused the primary crystal surface of ZIF-8 to begin to form [38,59,60]. In our study it was found that a similar rule can be applied to ZIF-67. Reducing the amount of deprotonated linker when the concentration of HMim is low (MR 1 to 8.8) limits the rate of nucleation and phase transformation [38]. Similarly, studies on ZIF-8 concluded that the crystal size and shape depend on both linker concentration and metal source and that crystals grow until they reach the thermodynamically more stable shape with the lowest surface energy. Different exposed crystallographic planes are present in each crystal form, and each crystallographic plane has a unique chemical composition [38,61]. Despite MR 6 did not exhibit the characteristic crystal shape of ZIF-67 but rather formed spherical crystal shape, it showed the characteristic XRD peaks of ZIF-67, as shown in Fig. 10b. This agrees with studies previously conducted on ZIF-8, which stated that different crystal structures might be composed of the same building blocks as ZIF-8 crystals despite having distinct topotactic phases [38].

The effect of molar ratio with fixed $Co(NO_3)_2$ concentration (=0.099 M) on the morphology of the ZIF-67 deposition was also determined via SEM images (Fig. 12, Fig. S16) in which again the molar ratio had profound effect on the shape of the crystals. Fig. 12 shows that rather than the characteristic crystal shape of ZIF-67, 1D rod (0.06 μm), petal (0.3×0.7 μm) and 3D rod (0.5×0.55 μm) crystals, were obtained for MR 1, 4 and 6, respectively. On the other hand, further increase in the molar, a continuous film of fused ZIF-67 crystals was formed at molar ratios of 8.8 and 16 with a thickness of 0.68 μm and 0.11 μm, respectively. This might be attributed to crystal growth by coalescence, a process when many nanoparticles assemble and fuse together [62] due to the high surface energy of such nanoparticles and their propensity to adhere to one another, lowering the particle's surface energy [63]. For the MR 16, a few large crystals were formed along the continuous film of ZIF-67. This might be attributed to that at this stage the crystal growth is due to that more precursor units adhere to the already formed nuclei and larger crystals are formed [62].

SEM images of HMim and cobalt nitrate are shown in Figs. S17 and

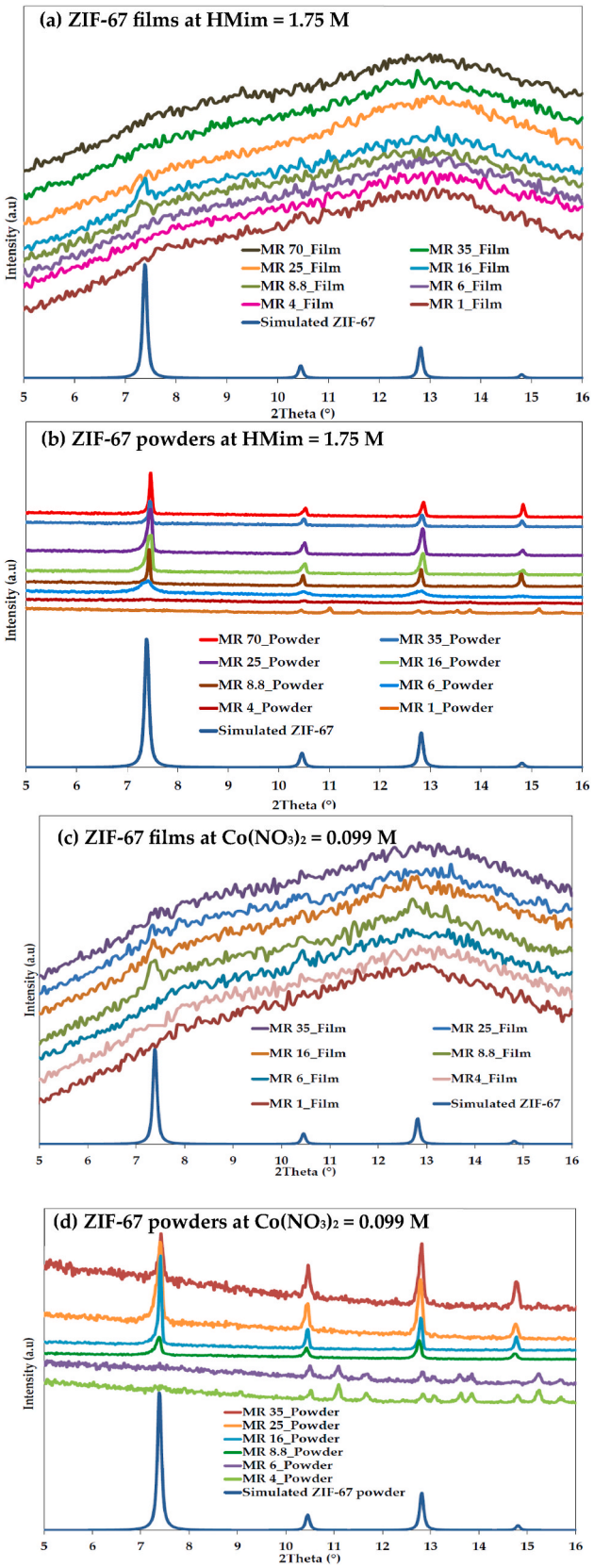

Fig. 10. XRD patterns of electrodeposited ZIF-67 a. films and b. powders at HMim concentration = 1.75 M, c. films and d. powders at cobalt nitrate concentration = 0.099 M at various molar ratios at −0.8 V for 10 min.

S18.

Similar results were observed in a study conducted on ZIF-8, where the molar ratio showed significant effect on the crystal shape [38]. In addition, crystals obtained at the same molar ratio (i.e., 6), but with different linker and metal concentrations can have different shapes such as spheres and rods for constant HMim and cobalt nitrate concentrations, respectively. The previous findings prove that there is a minimum concentration of precursors to obtain a fully developed crystal shape of ZIF-67. The average crystal size and surface coverage of the obtained ZIF-67 crystals are shown in Table 1. As the molar ratio was increased, the size of the ZIF-67 crystals increased. This may suggest that as the linker concentration increases, the solution becomes supersaturated. The supersaturation affects both the nucleation and crystal growth rates [64] as they both occur continuously and concurrently at the same time if the supersaturation level exceeds the critical nucleation threshold. Nevertheless, the greater thermodynamically favourable nuclei are formed when smaller nuclei redissolve and deposit onto them due to the Ostwald ripening, producing larger crystals [62].

Fig. S19a shows the FTIR spectrum of ZIF-67 powders formed at molar ratios between 1 and 70 when HMim concentration was 1.75 M. Although all the main bands of ZIF-67 crystals were observed for all molar ratios, some extra bands at 1015 cm^{-1} corresponding to C═C bending, 670 cm^{-1} and 1340 cm^{-1} for C–N stretching and 1560 cm^{-1} for N–O stretching were observed, respectively. This might suggest that structures formed at these molar ratios are made up of the same building units as fully developed ZIF-67 crystals despite that different topotactic phases are formed as previously concluded for ZIF-8 but with traces of the unreacted/protonated HMim and cobalt nitrate that prevented the full development of the right crystal structure [38]. Similar trend was observed in case of changing molar ratio when cobalt nitrate concentration was 0.099 M (Fig. S19b).

As ZIF-67 films could not been detected by XRD, XPS were measured for collected ZIF-67 powders from each experiment. Fig. S20 shows the wide scan and high-resolution scans of Co, N, C and O of the ZIF-67 developed using a reaction solution with a MR 8.8 at −0.8 V for 10 min (HMim concentration = 1.75 M).

The high-resolution XPS spectrum confirmed the Co–N bond which is characteristic feature for the formation of ZIF-67 as shown previously. The wide scan and high-resolution scans of Co, N, C and O of the ZIF-67 developed using a reaction solution with a MR 8.8 at −0.8 V for 10 min (cobalt nitrate concentration = 0.099 M) are shown in Fig. S21. The wide scan XPS spectra of the electrodeposited ZIF-67 at different molar ratio are shown in Fig. S22. It can be noticed that as the MR ratio changed, the composition of the formed phases changed accordingly.

Fig. S23 shows the cyclic voltammetry curves recorded for the ZIF-67 reaction solution at MR 8.8 for fixed cobalt nitrate and fixed HMim concentrations. Cyclic voltammetry is a valuable and convenient tool to monitor the changes in electrode surface properties [65]. It can be noticed that with in the investigated range there was no significant observed changes except a cathodic peak that can be attributed to hydrogen evolution. It can also be noticed that peak could not be observed for MR 8.8 fixed cobalt experiment. This could be attributed to the formation of a continuous film in case of the MR 8.8 fixed cobalt nitrate. A similar behaviour was observed and attributed to that the formation of films reducing the mobility of the charge carriers, and hence the conductivity [66].

3.4. Effect of solution pH

Our previous results concluded that the molar ratio has a profound effect on ZIF-67 deposition and crystal shape/morphology. In addition, as the molar ratio was changed, the pH and conductivity of the solution changed, which makes pH another crucial factor that affects the formation of ZIF-67. This is due to the deprotonation of the organic ligand and eventually the formation of MOF crystal structure. Fig. S26 shows the pale purple ZIF-67 layers on ITO/PET substrates, which were

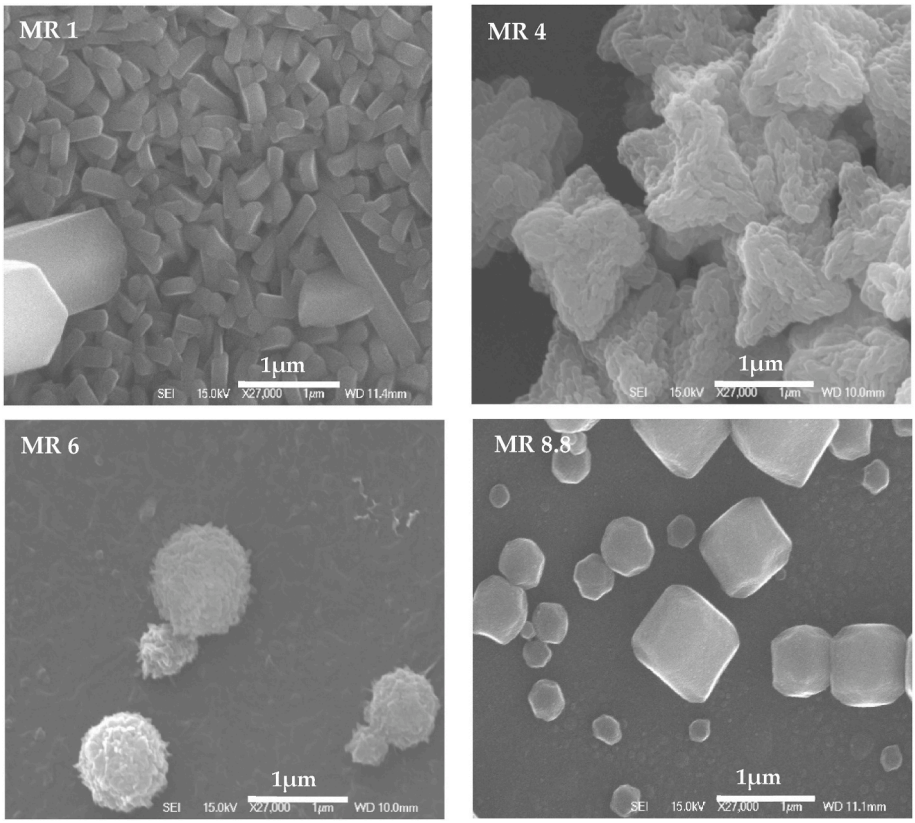

Fig. 11. SEM images of ZIF-67 depositions at molar ratios between 1 and 8.8 (HMim concentration = 1.75 M) at −0.8 V for 10 min.

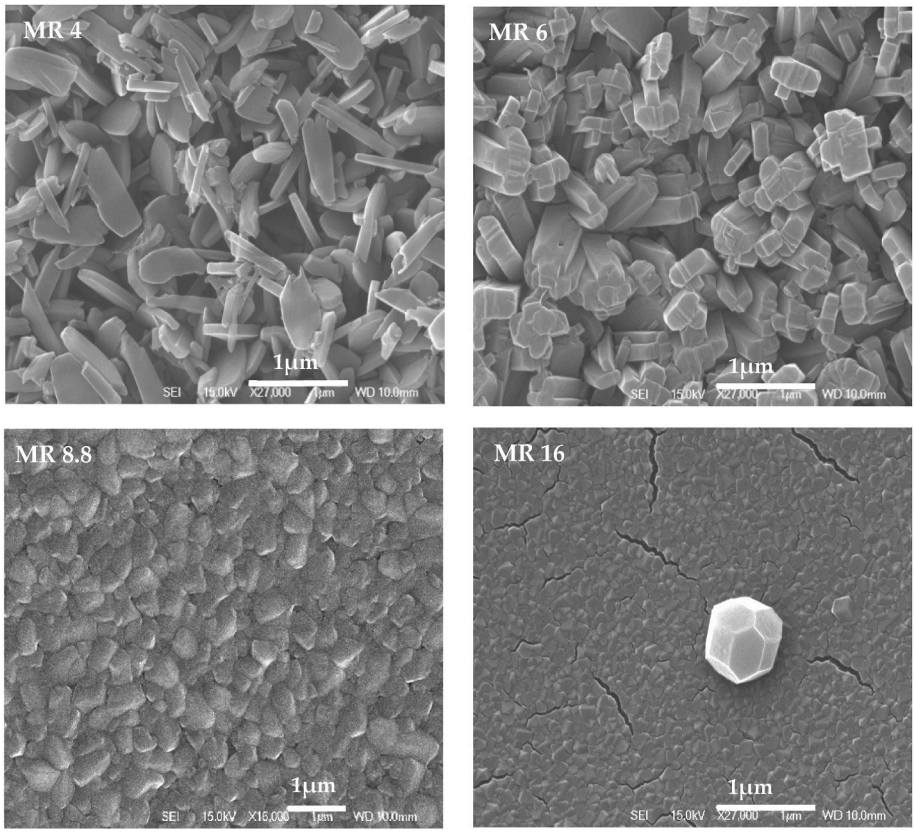

Fig. 12. SEM images of ZIF-67 films formed at molar ratios between 4 and 16 (Cobalt nitrate concentration = 0.099 M) at −0.8 V for 10 min.

Table 1
Effect of molar ratio on surface coverage and crystal size of ZIF-67.

Molar Ratio	Concentration (M)	ZIF-67 crystals	Average crystal size (μm)	Surface coverage (%)
8.83	**HMim: 1.75**	Yes	0.37 ± 0.1	25.77 ± 1.08
16			0.39 ± 0.14	22.45 ± 1.65
25			0.41 ± 0.14	15.8 ± 0.95
35			0.56 ± 0.16	14.35 ± 2.3
70			0.8 ± 0.18	10.18 ± 4.6
8.83	**$Co(NO_3)_2$: 0.099**	Yes	Film thickness 0.668 ± 0.05	Continuous coverage
16			Film thickness 0.11 ± 0.01	
25			0.169 ± 0.06	41.47 ± 0.9
35			0.1841 ± 0.03	77.68 ± 0.41

synthesized at various pH values. The very light purple colour can only be observed for the layers deposited from pH 9 to 11.6. Other substrates that were deposited at pH 7, 8 and 12.5 showed almost no signs of ZIF-67 on the substrates. Therefore, the XRD spectra were recorded for the powders collected at the bottom of the reaction vessel. Fig. 13 shows that all the characteristic peaks of ZIF-67 were observed for the powder samples collected at pH 9, 10, 11.6 and 12.5. In case of pH 7 and 8, no solids were collected. This supports the previous conclusion that the amount of the deprotonated linkers at lower pH values (<9) limits the rate of nucleation, phase transformation and crystal formation. This is due to that the low solution pH did not permit the deprotonation of HMim, formation of imidazolate ions and eventually nucleation and growth of the ZIF-67 crystals.

The effect of solution pH on the morphology of the ZIF-67 crystals on the substrates was determined via SEM images (Fig. 14). No crystals were observed via SEM at pH 7. Crystals found at pH 8 did not show the characteristic dodecahedron shape of ZIF-67 crystals but rather had a mixture of small rods and cubic shapes. This might be attributed to the fact that the concentration of imidazolate ions is not sufficiently high to be converted to ZIF-67 due to the limited deprotonation at such pH. At pH 9, the linker starts to deprotonate and produces imidazolate ions that coordinate with the cobalt ions to produce ZIF-67 crystals as evident from the XRD data (Fig. 13). At higher solution pH (11.6 and 12.5), a rapid deposition of ZIF-67 crystals in the bulk was noticed, specially at 12.5 (Fig. S27). This attributed to the fast deprotonation of HMim in the bulk of the solution demolishing the role of electrochemistry, justifying the low coverage of the substrates (Fig. 14). Also, ZIF-67 is known to have a positive surface charge as it has a positive zeta potential readings at pH ranges of 7 to 10, from 2.88 mV to 14.37 mV. With the addition of NaOH, the uncoordinated Co^{2+} sites at the outer surface of the ZIF-67

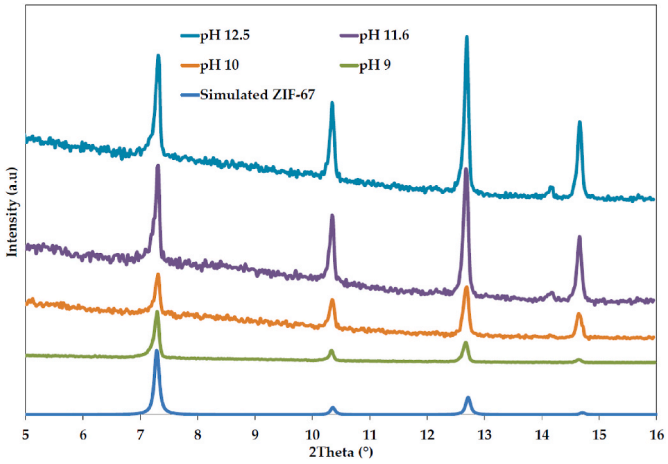

Fig. 13. XRD patterns of ZIF-67 powders collected at pH = 9–12.5 after electrodeposition for 10 min at −0.8 V.

bond with the hydroxyl group, neutralizing its charge and eventually making its zeta potential reach to zero. At this point, rapid precipitation takes place as shown in Fig. S27. The crystal sizes were ~ 0.25 μm, 0.29 μm, 0.32 μm and 0.46 μm for pH 9, 10, 11.6 and 12.5, respectively.

Fig. S28a shows the FTIR spectrum of ZIF-67 films formed on the ITO/PET substrates at various pH values. Due to the poor coverage of the substrates, the peak at 418 cm^{-1}, which is due the presence of the Co–N bond [67], is only visible for pH 10. On the other hand, the characteristic bands of ITO/PET substrate at 2970 and 1471 cm^{-1} were strongly evident for pH 7, 8 and 12.5 due to their poor ZIF-67 coverage. Fig. S28b shows the FTIR spectrum of ZIF-67 powders formed at various pH values. All the main bands of ZIF-67 were observed at all the investigated pH values. A band at 3136 cm^{-1} is only noticed for the powders collected at pH 9. This band is corresponding to the N–H stretching [68], which implies that the HMim was not fully coordinated with the cobalt ions as the band at 418 cm^{-1} is significantly strong [67]. This is supported with comparing the spectrum to HMim, where the same band can be observed.

As ZIF-67 films could not been detected by XRD, XPS were measured for the collected ZIF-67 powders from each experiment. Fig. S29 shows the wide scan and high-resolution scans of Co, N, C and O of the ZIF-67 developed at −0.8 V for 10 min at solution pH of 11.

The wide scan XPS spectra of the electrodeposited ZIF-67 at different solution pH are shown in Fig. S30. It should also be noted that a peak of NaKL1 appeared in case of pH 11.6 and 12.5 which can be attributed to using NaOH in adjusting the solution pH.

To determine whether linker/metal ratio or pH of the solution has more pronounced effect on the formation of ZIF-67 crystals, experiments were repeated for MR1 (solution pH = 8.4) and MR16 (solution pH = 9.7) (cobalt concentration = 0.99 M) after their pH adjustment. Previously, at MR1, no solids were formed and thus pH value was increased to 11 by using NaOH solution. For MR16, where continuous film formation was observed, solution pH was reduced from 9.7 to 8.4. With increasing the solution pH of the MR1, some powder was collected.

Fig. 15a shows the XRD patterns and SEM images of MR1 and MR16, comparing with and without pH adjustments. The peaks at 19°, 32° and 38° in the XRD patterns for MR1 after pH adjustment matches the peaks of cobalt hydroxide, shown in previous studies [69,70]. Even though the pH was sufficiently high to deprotonate HMim, ZIF-67 did not form from MR1 solution but rather cobalt hydroxide as also supported from Fig. 15b. This supports similar conclusion that there is a minium concentration of HMim to allow the formation of ZIF-67. At pH > 9, the solubility of cobalt species significantly decreases and precipitation takes place [71]. The unreacted HMim was removed through the successive washing procedures as no characteristic peaks were observed.

Regarding the MR16 pH adjustment, SEM images showed that rather than a continous layer of ZIF-67 that was previously formed, individual crystals were formed on the substrate (Fig. 15c). Even though the HMim concentration was high, the low pH did not allow the full deprotonation of HMim and hence ZIF-67 formation was restricted. SEM images also exhibited crystal etching due to the use of concentrated HNO_3. The Co–N bonds are broken and the acid slowly carves the external crystal surfaces [61]. Again, the unreacted HMim was removed through the successive washing procedures. These results imply that both solution pH and linker/metal molar ratio have important roles in the formation of ZIF-67, however, the latter is more predominant as the ratio controls nucleation step at first place. This may suggest that even if the pH is sufficiently high to deprotonate the linker, nucleation might not take place when the linker concentration is not high enough to coordinate with the metal ion. Nevertheless, the pH will become more important once the reactants' concentrations are high enough to form the ZIF-67 nuclei.

4. Conclusions

In this study, ZIF-67 was synthesized using cathodic electrochemical

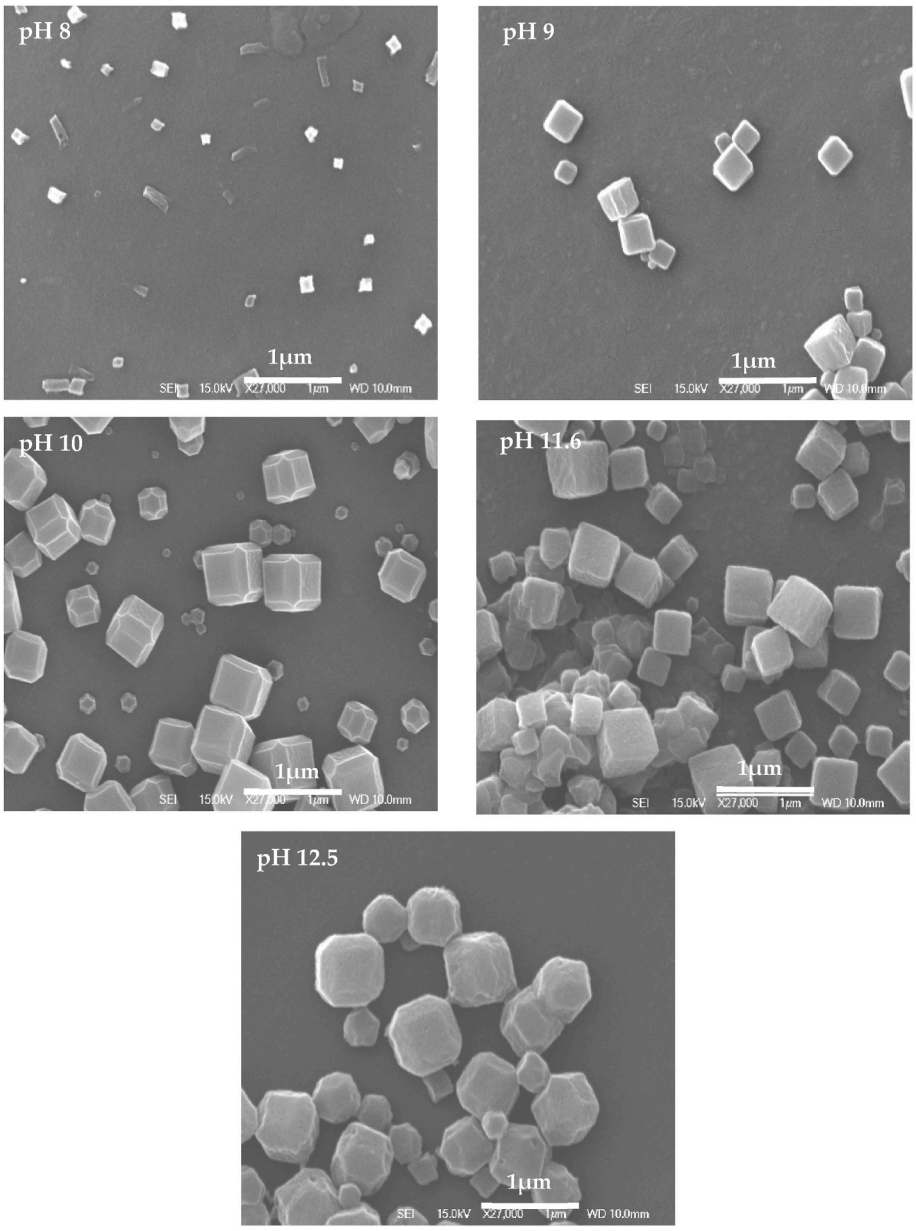

Fig. 14. SEM images of ZIF-67 crystals electrodeposited at various pH values at −0.8 V for 10 min.

deposition technique on ITO/PET substrate using water as a solvent. Operating parameters such as applied potential (−0.25 to −0.8V), solution pH (7 to 12.5) and linker/metal molar ratio (MR = 1 to 70) were investigated. Results revealed that increasing the applied potential from −0.25 V to −0.8 V, increased the surface coverage from 19.7 % ± 1.45 to 45.6 % ± 0.68 and decreased the crystal size from 0.52 ± 0.1 μm to 0.29 ± 0.1 μm. A further increase in the applied potential affected the electrical properties of the substrate and hence −0.8 V was chosen as the optimum potential.

Changing the linker/metal molar ratio had a profound effect on the shape and size of the formed crystals. The characteristic ZIF-67 crystals formed when the MR is > 6. Continuous films of ZIF-67 with thicknesses of 0.66 and 0.11 μm were formed with MRs between 8.8 and 16, at cobalt nitrate concentration of 0.099 M. Solution pH had a significant effect on the deprotonation of the organic linker and thus ZIF-67 was only formed at pH > 9. Excessive increase in the pH caused the precipitation of ZIF-67 in the solution bulk rather than on the substrate. Our statistical analyses also showed low p-values (≪0.05), expressing strong relation between variables and robustness and reliability of the data collected in this study. Finally, mathematical expressions were fitted to experimental data to reveal the relationship between applied potential, molar ratios of reactants, pH and conductivity of solutions, surface coverage and crystal size. This study paves the way to control the crystal size and shape of electrochemically synthesized ZIF-67 using water as solvent.

CRediT authorship contribution statement

Eman Elsayed: Writing – review & editing, Writing – original draft, Visualization, Validation, Methodology, Investigation, Conceptualization, Data curation. **Ignacio Brevis:** Data curation, Investigation, Methodology. **Sathish Pandiyan:** Investigation, Methodology. **Ricky Wildman:** Funding acquisition, Project administration, Resources. **Kristoffer G. van der Zee:** Funding acquisition, Project administration, Resources. **Begum Tokay:** Writing – review & editing, Visualization, Validation, Supervision, Resources, Project administration, Methodology, Investigation, Funding acquisition.

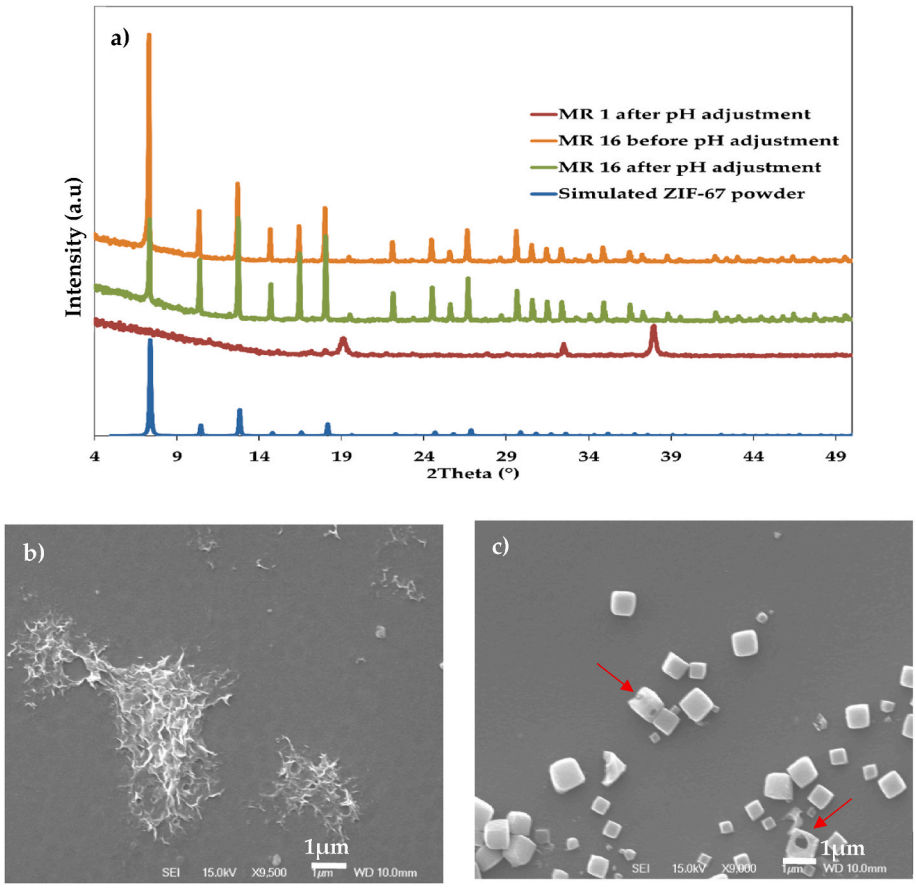

Fig. 15. a. XRD patterns and SEM images of formed crystal on substrate after pH adjustment of b. MR1 and c. MR16 at −0.8 V for 10 min (Red arrows point at etched crystals).

Declaration of competing interest

The authors declare that they have no known competing financial interests or personal relationships that could have appeared to influence the work reported in this paper.

Data availability

Data will be made available on request.

5. Acknowledgements

The authors would like to thank the Engineering and Physical Sciences Research Council (EPSRC) for financially funding this work (Grant Ref: EP/W010011/1). Also, authors would like to thank the Nanoscale and Microscale Research Centre (nmRC) and Materials Engineering (Wolfson Building), University of Nottingham for providing access to characterization instruments.

Appendix A. Supplementary data

Supplementary data to this article can be found online at https://doi.org/10.1016/j.jssc.2024.124820.

References

[1] S. Dutt, A. Kumar, S. Singh, Synthesis of metal organic frameworks (MOFs) and their derived materials for energy storage applications, Cleanroom Technol. 5 (1) (2023) 140–166.
[2] O.K. Akeremale, O.T. Ore, A.A. Bayode, H. Badamasi, J.A. Olusola, S.S. Durodola, Synthesis, characterization, and activation of metal organic frameworks (MOFs) for the removal of emerging organic contaminants through the adsorption-oriented process: a review, Results Chem. 5 (2023) 100866.
[3] H.E. Emam, H.B. Ahmed, M. El-Shahat, H. Abdel-Gawad, R.M. Abdelhameed, Selective separation of chlorophyll-a using recyclable hybrids based on Zn-MOF@cellulosic fibers, Sci. Rep. 13 (1) (2023) 15208.
[4] H.E. Emam, R.M. Abdelhameed, Separation of anthocyanin from roselle extract by cationic nano-rode ZIF-8 constructed using removable template, J. Mol. Struct. 1267 (2022) 133607.
[5] H.E. Emam, M. El-Shahat, M. Taha, R.M. Abdelhameed, Microwave assisted post-synthetic modification of IRMOF-3 and MIL-68-NH2 onto cotton for Fuel purification with computational explanation, Surface. Interfac. 30 (2022) 101940.
[6] R.M. Abdelhameed, M. Hasanin, H. Abdel-Gawad, B. Hegazi, Engineering ZIF-8 hybridization by extracted lignin with antibacterial property for uptake of methomyl residues from wastewater, Separ. Sci. Technol. 57 (18) (2022) 3023–3034.
[7] G. Zhong, D. Liu, J. Zhang, The application of ZIF-67 and its derivatives: adsorption, separation, electrochemistry and catalysts, J. Mater. Chem. A 6 (5) (2018) 1887–1899.
[8] Z. Feng, H. Lim, I. Ibrahim, N. Gowthaman, A review of zeolitic imidazolate frameworks (ZIFs) as electrochemical sensors for important small biomolecules in human body fluids, J. Mater. Chem. B 11 (38) (2023) 9099–9127.
[9] X. Guo, T. Xing, Y. Lou, J. Chen, Controlling ZIF-67 crystals formation through various cobalt sources in aqueous solution, J. Solid State Chem. 235 (2016) 107–112.
[10] M.N. Timofeeva, V.N. Panchenko, S.H. Jhung, Insights into the structure–property–activity relationship of zeolitic imidazolate frameworks for acid–base catalysis, Int. J. Mol. Sci. 24 (5) (2023) 4370.
[11] C. Duan, Y. Yu, H. Hu, Recent progress on synthesis of ZIF-67-based materials and their application to heterogeneous catalysis, Green Energy Environ. 7 (1) (2022) 3–15.
[12] C. Duan, F. Li, M. Yang, H. Zhang, Y. Wu, H. Xi, Rapid synthesis of hierarchically structured multifunctional metal–organic zeolites with enhanced volatile organic compounds adsorption capacity, Ind. Eng. Chem. Res. 57 (45) (2018) 15385–15394.
[13] X. Wu, W. Liu, H. Wu, X. Zong, L. Yang, Y. Wu, Y. Ren, C. Shi, S. Wang, Z. Jiang, Nanoporous ZIF-67 embedded polymers of intrinsic microporosity membranes with enhanced gas separation performance, J. Membr. Sci. 548 (2018) 309–318.

[14] C. Wang, F. Yang, L. Sheng, J. Yu, K. Yao, L. Zhang, Y. Pan, Zinc-substituted ZIF-67 nanocrystals and polycrystalline membranes for propylene/propane separation, Chem. Commun. 52 (85) (2016) 12578–12581.
[15] R. Wu, Y. Li, A. Huang, Synthesis of high-performance Co-based ZIF-67 membrane for H2 separation by using cobalt ions chelated PIM-1 as interface layer, J. Membr. Sci. 620 (2021) 118841.
[16] Z. Zhao, L. Ding, R. Hinterding, A. Mundstock, C. Belke, R.J. Haug, H. Wang, A. Feldhoff, MXene assisted preparation of well-intergrown ZIF-67 membrane for helium separation, J. Membr. Sci. 652 (2022) 120432.
[17] Z. Wang, Y. Lu, Y. Yan, T.Y.P. Larissa, X. Zhang, D. Wuu, H. Zhang, Y. Yang, X. Wang, Core-shell carbon materials derived from metal-organic frameworks as an efficient oxygen bifunctional electrocatalyst, Nano Energy 30 (2016) 368–378.
[18] B. Li, K. Igawa, J. Chai, Y. Chen, Y. Wang, D.W. Fam, N.N. Tham, T. An, T. Konno, A. Sng, String of pyrolyzed ZIF-67 particles on carbon fibers for high-performance electrocatalysis, Energy Storage Mater. 25 (2020) 137–144.
[19] H. Wang, Q. He, S. Liang, Y. Li, X. Zhao, L. Mao, F. Zhan, L. Chen, Advances and perspectives of ZIFs-based materials for electrochemical energy storage: design of synthesis and crystal structure, evolution of mechanisms and electrochemical performance, Energy Storage Mater. 43 (2021) 531–578.
[20] J. Wang, I. Imaz, D. Maspoch, Metal– organic frameworks: why make them small? Small Struct. 3 (1) (2022) 2100126.
[21] M. Li, M. Dinca, Reductive electrosynthesis of crystalline metal–organic frameworks, J. Am. Chem. Soc. 133 (33) (2011) 12926–12929.
[22] N. Campagnol, T.R. Van Assche, M. Li, L. Stappers, M. Dincă, J.F. Denayer, K. Binnemans, D.E. De Vos, J. Fransaer, On the electrochemical deposition of metal–organic frameworks, J. Mater. Chem. A 4 (10) (2016) 3914–3925.
[23] S. Xiong, X. Qian, Z. Zhong, Y. Wang, Atomic layer deposition for membrane modification, functionalization and preparation: a review, J. Membr. Sci. (2022) 120740.
[24] S. Majumdar, B. Tokay, V. Martin-Gil, J. Campbell, R. Castro-Muñoz, M.Z. Ahmad, V. Fila, Mg-MOF-74/Polyvinyl acetate (PVAc) mixed matrix membranes for CO2 separation, Separ. Purif. Technol. 238 (2020) 116411.
[25] J. Warfsmann, B. Tokay, N.R. Champness, Synthesis of MIL-53 thin films by vapour-assisted conversion, CrystEngComm 22 (6) (2020) 1009–1017.
[26] E. Aliyev, J. Warfsmann, B. Tokay, S. Shishatskiy, Y.-J. Lee, J. Lillepaerg, N. R. Champness, V. Filiz, Gas transport properties of the metal–organic framework (MOF)-assisted polymer of intrinsic microporosity (PIM-1) thin-film composite membranes, ACS Sustain. Chem. Eng. 9 (2) (2020) 684–694.
[27] J. Campbell, B. Tokay, Controlling the size and shape of Mg-MOF-74 crystals to optimise film synthesis on alumina substrates, Microporous Mesoporous Mater. 251 (2017) 190–199.
[28] C. Crivello, S. Sevim, O. Graniel, C. Franco, S. Pané, J. Puigmartí-Luis, D. Muñoz-Rojas, Advanced technologies for the fabrication of MOF thin films, Mater. Horiz. 8 (1) (2021) 168–178.
[29] S. Xie, W. Monnens, K. Wan, W. Zhang, W. Guo, M. Xu, I.F. Vankelecom, X. Zhang, J. Fransaer, Cathodic electrodeposition of MOF films using hydrogen peroxide, Angew. Chem. Int. Ed. 60 (47) (2021) 24950–24957.
[30] H. Zhu, H. Liu, I. Zhitomirsky, S. Zhu, Preparation of metal–organic framework films by electrophoretic deposition method, Mater. Lett. 142 (2015) 19–22.
[31] I. Stassen, M. Styles, T. Van Assche, N. Campagnol, J. Fransaer, J. Denayer, J.-C. Tan, P. Falcaro, D. De Vos, R. Ameloot, Electrochemical film deposition of the zirconium metal–organic framework UiO-66 and application in a miniaturized sorbent trap, Chem. Mater. 27 (5) (2015) 1801–1807.
[32] A. Walcarius, E. Sibottier, M. Etienne, a. Ghanbaja, Electrochemically assisted self-assembly of mesoporous silica thin films, Nat. Mater. 6 (8) (2007) 602–608.
[33] C. Yu, Y. Liang, W. Xue, Z. Zhang, X. Jia, H. Huang, Z. Qiao, D. Mei, C. Zhong, Polymer-supported ultra-thin ZIF-67 membrane through in situ interface self-repair, J. Membr. Sci. 625 (2021) 119139.
[34] D. Sun, D. Yang, P. Wei, B. Liu, Z. Chen, L. Zhang, J. Lu, One-step electrodeposition of silver nanostructures on 2D/3D metal–organic framework ZIF-67: comparison and application in electrochemical detection of hydrogen peroxide, ACS Appl. Mater. Interfaces 12 (37) (2020) 41960–41968.
[35] Z. Li, J. Cui, Y. Liu, J. Li, K. Liu, M. Shao, Electrosynthesis of well-defined metal–organic framework films and the carbon nanotube network derived from them toward electrocatalytic applications, ACS Appl. Mater. Interfaces 10 (40) (2018) 34494–34501.
[36] P. Zhou, J. Cheng, Y. Yan, S. Xu, C. Zhou, Ultrafast preparation of hydrophobic ZIF-67/copper mesh via electrodeposition and hydrophobization for oil/water separation and dyes adsorption, Separ. Purif. Technol. 272 (2021) 118871.
[37] P.M. Usov, C. McDonnell-Worth, F. Zhou, D.R. MacFarlane, D.M. D'Alessandro, The electrochemical transformation of the zeolitic imidazolate framework ZIF-67 in aqueous electrolytes, Electrochim. Acta 153 (2015) 433–438.
[38] M. Jian, B. Liu, R. Liu, J. Qu, H. Wang, X. Zhang, Water-based synthesis of zeolitic imidazolate framework-8 with high morphology level at room temperature, RSC Adv. 5 (60) (2015) 48433–48441.
[39] T.R. Van Assche, G. Desmet, R. Ameloot, D.E. De Vos, H. Terryn, J.F. Denayer, Electrochemical synthesis of thin HKUST-1 layers on copper mesh, Microporous Mesoporous Mater. 158 (2012) 209–213.
[40] M. Mozafari, Metal-organic Frameworks for Biomedical Applications, Woodhead Publishing, 2020.
[41] X. Zhang, K. Wan, P. Subramanian, M. Xu, J. Luo, J. Fransaer, Electrochemical deposition of metal–organic framework films and their applications, J. Mater. Chem. A 8 (16) (2020) 7569–7587.
[42] S. Zhou, O. Shekhah, J. Jia, J. Czaban-Jóźwiak, P.M. Bhatt, A. Ramírez, J. Gascon, M. Eddaoudi, Electrochemical synthesis of continuous metal–organic framework membranes for separation of hydrocarbons, Nat. Energy 6 (9) (2021) 882–891.
[43] S.D. Worrall, H. Mann, A. Rogers, M.A. Bissett, M.P. Attfield, R.A. Dryfe, Electrochemical deposition of zeolitic imidazolate framework electrode coatings for supercapacitor electrodes, Electrochim. Acta 197 (2016) 228–240.
[44] S.D. Worrall, Anodic Deposition of Metal-Organic Framework Coatings for Electrochemical Applications, The University of Manchester, United Kingdom, 2017.
[45] P. Zhou, Y. Yan, J. Cheng, C. Zhou, Stainless steel mesh coated with defect engineered ZIF-67 toward pH-switchable wettability and efficient organic liquids separation, Colloids Surf. A Physicochem. Eng. Asp. 634 (2022) 127950.
[46] K. Yin, H. Zhang, Y. Yan, High efficiency of toluene adsorption over a novel ZIF-67 membrane coating on paper-like stainless steel fibers, J. Solid State Chem. 279 (2019) 120976.
[47] N. Fairley, V. Fernandez, M. Richard-Plouet, C. Guillot-Deudon, J. Walton, E. Smith, D. Flahaut, M. Greiner, M. Biesinger, S. Tougaard, Systematic and collaborative approach to problem solving using X-ray photoelectron spectroscopy, Appl. Surf. Sci. Adv. 5 (2021) 100112.
[48] C. Sun, J. Yang, X. Rui, W. Zhang, Q. Yan, P. Chen, F. Huo, W. Huang, X. Dong, MOF-directed templating synthesis of a porous multicomponent dodecahedron with hollow interiors for enhanced lithium-ion battery anodes, J. Mater. Chem. A 3 (16) (2015) 8483–8488.
[49] J. Bahar, Y. Lghazi, B. Youbi, M. Ait Himi, I. Bimaghra, Comparative study of nucleation and growth mechanism of cobalt electrodeposited on ITO substrate in nitrate and chloride electrolytes, J. Solid State Electrochem. 25 (6) (2021) 1889–1900.
[50] Y. Zhang, H. Xu, Y. Jia, X. Yang, M. Gao, Snowflake Cu2S@ ZIF-67: a novel heterostructure substrate for enhanced adsorption and sensitive detection in SERS, J. Hazard Mater. (2024) 134524.
[51] M. Varsha, G. Nageswaran, Direct electrochemical synthesis of metal organic frameworks, J. Electrochem. Soc. 167 (15) (2020) 155527.
[52] Ö.H. Demirel, T. Rijnaarts, P. de Wit, J.A. Wood, N.E. Benes, Electroforming of a metal–organic framework on porous copper hollow fibers, J. Mater. Chem. A 7 (20) (2019) 12616–12626.
[53] W.-J. Li, J. Lü, S.-Y. Gao, Q.-H. Li, R. Cao, Electrochemical preparation of metal–organic framework films for fast detection of nitro explosives, J. Mater. Chem. A 2 (45) (2014) 19473–19478.
[54] M. Shahsavari, M. Mortazavi, S. Tajik, I. Sheikhshoaie, H. Beitollahi, Synthesis and characterization of GO/ZIF-67 nanocomposite: investigation of catalytic activity for the determination of epinine in the presence of dobutamine, Micromachines 13 (1) (2022) 88.
[55] M. Shahmirzaee, A. Hemmati-Sarapardeh, M.M. Husein, M. Schaffie, M. Ranjbar, Development of a powerful zeolitic imidazolate framework (ZIF-8)/carbon fiber nanocomposite for separation of hydrocarbons and crude oil from wastewater, Microporous Mesoporous Mater. 307 (2020) 110463.
[56] M. Senthilkumar, J. Mathiyarasu, J. Joseph, K. Phani, V. Yegnaraman, Electrochemical instability of indium tin oxide (ITO) glass in acidic pH range during cathodic polarization, Mater. Chem. Phys. 108 (2–3) (2008) 403–407.
[57] Y. Wu, Y. Wang, Z. Xiao, M. Li, Y. Ding, M.-l. Qi, Electrocatalytic oxygen reduction by a Co/Co 3 O 4@ N-doped carbon composite material derived from the pyrolysis of ZIF-67/poplar flowers, RSC Adv. 11 (5) (2021) 2693–2700.
[58] R.K. Devi, G. Muthusankar, S.-M. Chen, G. Gopalakrishnan, In situ formation of Co3O4 nanoparticles embedded N-doped porous carbon nanocomposite: a robust material for electrocatalytic detection of anticancer drug flutamide and supercapacitor application, Microchim. Acta 188 (6) (2021) 196.
[59] J.H. Park, J. Paczesny, N. Kim, B.A. Grzybowski, Shaping microcrystals of metal–organic frameworks by reaction–diffusion, Angew. Chem. Int. Ed. 59 (26) (2020) 10301–10305.
[60] X. Wang, C. Liu, B. Zheng, Y. Jiang, L. Zhang, Z. Xie, L. Zheng, Controlled synthesis of concave Cu 2 O microcrystals enclosed by {hhl} high-index facets and enhanced catalytic activity, J. Mater. Chem. A 1 (2) (2013) 282–287.
[61] J. Cravillon, S. Münzer, S.-J. Lohmeier, A. Feldhoff, K. Huber, M. Wiebcke, Rapid room-temperature synthesis and characterization of nanocrystals of a prototypical zeolitic imidazolate framework, Chem. Mater. 21 (8) (2009) 1410–1412.
[62] Z. Shi, Y. Yu, C. Fu, L. Wang, X. Li, Water-based synthesis of zeolitic imidazolate framework-8 for CO 2 capture, RSC Adv. 7 (46) (2017) 29227–29232.
[63] C. Avci, J. Ariñez-Soriano, A. Carné-Sánchez, V. Guillerm, C. Carbonell, I. Imaz, D. Maspoch, Post-synthetic anisotropic wet-chemical etching of colloidal sodalite ZIF crystals, Angew. Chem. 127 (48) (2015) 14625–14629.
[64] P.W. Dunne, A.S. Munn, C.L. Starkey, T.A. Huddle, E.H. Lester, Continuous-flow hydrothermal synthesis for the production of inorganic nanomaterials, Phil. Trans. Math. Phys. Eng. Sci. 373 (2057) (2015) 20150015.
[65] A.A. Tezerjani, R. Halladj, S. Askari, Different view of solvent effect on the synthesis methods of zeolitic imidazolate framework-8 to tuning the crystal structure and properties, RSC Adv. 11 (32) (2021) 19914–19923.
[66] A. Hussein, Essentials of Flow Assurance Solids in Oil and Gas Operations: Understanding Fundamentals, Characterization, Prediction, Environmental Safety, and Management, 2022. Gulf Professional Publishing.
[67] R. Bogdanowicz, P. Niedziałkowski, M. Sobaszek, D. Burnat, W. Białobrzeska, Z. Cebula, P. Sezemsky, M. Koba, V. Stranak, T. Ossowski, Optical detection of ketoprofen by its electropolymerization on an indium tin oxide-coated optical fiber probe, Sensors 18 (5) (2018) 1361.
[68] N. Joshi, K. Rawat, P.R. Solanki, H. Bohidar, Biocompatible laponite ionogels based non-enzymatic oxalic acid sensor, Sens.and Bio-Sens.Res. 5 (2015) 105–111.

[69] X.-D. Du, C.-C. Wang, J.-G. Liu, X.-D. Zhao, J. Zhong, Y.-X. Li, J. Li, P. Wang, Extensive and selective adsorption of ZIF-67 towards organic dyes: performance and mechanism, J. Colloid Interface Sci. 506 (2017) 437–441.
[70] H. Wan, J. Wang, X. Sheng, J. Yan, W. Zhang, Y. Xu, Removal of polystyrene microplastics from aqueous solution using the metal–organic framework material of ZIF-67, Toxics 10 (2) (2022) 70.
[71] R. Ediati, P. Elfianuar, E. Santoso, D.O. Sulistiono, M. Nadjib, Synthesis of MCM-41/ZIF-67 composite for enhanced adsorptive removal of methyl orange in aqueous solution. Mesoporous Materials-Properties and Applications, 2019, pp. 1–14.